COVID-I Net: Towards Computer-Aided assessment Of Covid-19 Effect on Lung Infection severity via Deep Neural Networks For Chest X-Rays And CT Scan Images

Rajeshkumar K[1], Karthikeyan V.[2], Prasanna Venkatesan A.[3], Shanmuganathan M[4]
[1, 2, 3] Dept of of Computer Science and Engineering
[4]Assistant Professor, Dept of of Computer Science and Engineering
[1, 2, 3, 4] Panimalar Engineering College, Chennai, Tamil Nadu, India

Abstract- *COVID-19 pandemic is affecting numerous lives all around the world. Effective care and treatment planning for COVID-19 infected patients are mandatory. This infectious virus caused by severe acute respiratory syndrome corona virus 2 (SARS-CoV-2) requires primary investigation to access infection severity progression. The assessment metrics of COVID-19 infected patients involve lung involvement and opacity extent from CXR (Chest X-ray images) and CT scan. CXR (Chest x-ray images) are preferred over CT scans because of inferring a feasibly possible solution available to infected patients. We also analyzed CT scans of infected individuals to gain insights on progression. The proposed model (COVID-19 I-NET a deep convolution neural network) using U-NET architecture resulted in image segmentation of infected areas from CXR and CT scan images. A system-aided method is used for the assignment of scores to infection severity and progression on CXR. Deep learning neural architecture such as U-NET, PSP NET, and SEG NET are evaluated and tabulated upon CXR and CT scan images. The segmentation results are promising and leading to be used as a tool for accessing image segmentation, heat map, lung area progression, and opacity of infected regions.*

Keywords- COVID-19, Pneumonia, SegNet, U-NET, PSP-NET, Computerized tomography, Semantic segmentation, Image analysis.

I. INTRODUCTION

COVID-19 is a fast-spreading disease that is causing thousands of deaths daily, all over the world. Early diagnosis of this disease proved to be one of the most effective methods for disease control. A large number of COVID-19 patients is rendering health care systems in many countries, overwhelmed. Hence, automation of identifying and analysing the infected lung regions would be really important. The RT-PCR (Real-Time Reverse Transcription-Polymerase Chain Reaction is being followed as the standard approach for COVID-19[1-2] screening. RT-PCR can detect the viral RNA in specimens obtained by nasopharyngeal swab, oropharyngeal swab, Broncho alveolar lavage, or tracheal aspirate. However, a variety of recent studies indicate that RT-PCR testing suffers from low sensitivity, approximately around 71%, whereby repeated testing is needed for accurate diagnosis. Furthermore, RT-PCR screening is time-consuming and has increasing availability limitations due to a shortage of required material. An alternative solution to RT-PCR for COVID-19 screening in medical imaging like X-ray or computed tomography (CT). Medical imaging technology has made significant progress in recent years and is now a commonly used method for diagnosis, as well as for quantification assessment of numerous diseases. The chest CT screening is a routine diagnostic tool for pneumonia around the world. Since both COVID-19 and Pneumonia are known to infect the lungs mainly, chest CT imaging[3-5] has been recommended for COVID-19 diagnosis. In addition, CT imaging is playing an important role in COVID-19 severity assessment, as well as disease monitoring.

COVID-19 infected areas can be identified on CT images by ground-glass opacity (GGO) in the early infection stage and by pulmonary consolidation in the late infection stage. In comparison to the RT-PCR test, several studies showed that a CT scan is more sensitive and effective for COVID-19 screening [6-10]even without the occurrence of clinical symptoms. Even though increasing CT scan resolution and number of slices resulted in higher sensitivity and accuracy, these improvements also increased the workload. Also, annotations of medical images are often influenced by clinical experience. Automated medical image analysis could be a better solution for these challenges. The field of Image segmentation has been developing rapidly with the development of advanced deep-learning methods in Artificial Intelligence.

Radiologists have identified three types of irregularities related to COVID-19 in Computed Tomography (CT) lung images: Ground Glass Opacification (GGO), Consolidation, and pleural effusion. Developing an automated tool for semantically segmenting the CT scanned lung images of infected patients would contribute and help in quantifying these three irregularities. It will be a breakthrough in this pandemic to better manage the situation in overloaded hospitals. Deep learning (DL)[11-15]has become a conventional method for constructing networks capable of successfully modelling higher-order systems to achieve human-like performance. Tumours have been direct targets for DL-assisted segmentation of medical images. A lung cancer screening tool was implemented using DL structures aiming to lower the false positive rate in lung cancer screening with low-dose CT scans.

Many research projects have been conducted for COVID-19 detection using deep learning techniques in image analysis of X-Ray and CT scans[16-18] and they have given remarkable results. Yet, detailed segmentation of those images has been less appealing. A recent study designed a binary classifier (COVID-19, No information) and a multi classifier (COVID-19, No Information, Pneumonia) using a CNN with X-Ray images as an input, reaching an output of 0.98 for binary classes and 0.87 for a multi-class classifier for COVID-19 severity detection. Another study used Xception and ResNet50V2 networks, resulting in an accuracy of 0.99 for the target class.

The aim of medical image segmentation (MIS) is the automated identification and labelling of regions of interest (ROI) e.g. organs like lungs or medical abnormalities like cancer and lesions. In recent studies, medical image segmentation models based on neural networks proved powerful prediction capabilities and achieved similar results as radiologists regarding performance. It would be a helpful tool to implement such an automatic segmentation for COVID-19 infected regions as clinical decision support for physicians. By automatically highlighting abnormal features and ROIs, image segmentation can aid radiologists in diagnosis, disease course monitoring, and reduction of time-consuming inspection processes, and improvement of accuracy. Nevertheless, training accurate and robust models requires sufficient annotated medical imaging data. Because manual annotation is labour-intensive, time-consuming, and requires experienced radiologists, it is common that publicly available data is limited. This lack of data often results in overfitting of the traditional data-hungry models. Especially for COVID-19, large enough medical imaging datasets are currently unavailable.

In this work, we push towards creating an accurate and state-of-the-art MIS pipeline for COVID-19 lung infection segmentation, which is capable of being trained on small datasets consisting of CT volumes and x-ray. To avoid overfitting, we exploit extensive on-the-fly data augmentation, as well as diverse pre-processing methods. To further reduce the risk of overfitting, we implement the standard U-Net architecture, PSP, SEGNET. Moreover, we use 5-step cross-validation for reliable performance evaluation. Implementing such a validation method would be a key component in a system that prioritizes patients by severity of infection. It would identify an infection and output its key spatial features such as location, distribution, and shape parameters[19-21].Bounding-box segments, by definition, fail to deliver such parameters[22-25].

II. MATERIALS AND METHODS

2.1. Dataset preparation:

2.1.1. Chest X-ray (CXR) Images:

The primary goal of this study is to assess the feasibility of automated severity scoring of COVID-19 using deep learning techniques. We develop and evaluate deep neural networks that can score Chest X-Rays of patients with COVID-19. Data consisted of CXR data about COVID-19 positive cases. The 396 CXR images used here represent a patient population of 267 patients between 12 and 88 years old around the world. The CXR data were acquired using a range of X-ray imaging equipment types and acquisition protocols that are representative of routine imaging practice (including supine and upright, posterior-anterior, and anterior-posterior).

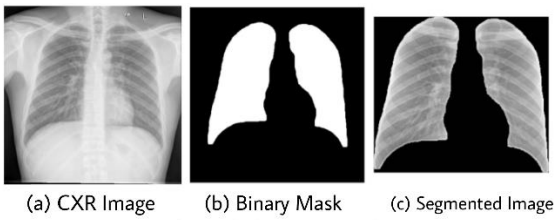

Fig 1: CXR Dataset with Masked and Segmented Lung images.

2.1.2. CT Scan Images:

Images of the dataset used in this work are a publicly available collection of the Italian Society of Medical and Interventional Radiology. A hundred one-slice CT scans are provided in a resized 512 × 512 dimensions. Region labels are already compiled into a NIFTI with proper documentation. In manual labelling, classes pixel count (total number of pixels in

a class) and image pixel count (total number of pixels in images that had an instance of a class) show an extensive disparity in representation; the dominant class is larger in order of 1e+3 than the least represented class. See Table 1. In this, the class C0 not only represent unaffected lung areas by pneumonia, but also the lung-enclosing tissue. The dataset source offers image masks for the segmentation of the lung regions. These masks were created automatically based on. The automated lung segmentation model can be found in the GitHub repository JoHo/lung mask.

Figure 2 illustrates the original, the lung-masked, and the labelled images of one sample.

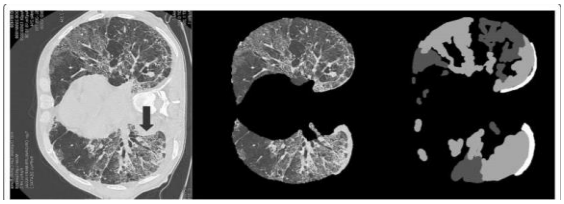

Fig 2: CT scan (left), Masked image (Middle) and labelled class (Right)

By seeing the dataset images, we can notice that the infected areas of the lungs are present in specific regions. To illustrate the correlation between infected tissue and its relative location, all the labels of the dataset were summed and plotted with a hot colour map in Fig.3. From the accumulation image, we can confirm that some parts of the lungs are more prone to infection. Thus, the spatial values of pixels are a key feature in this research.

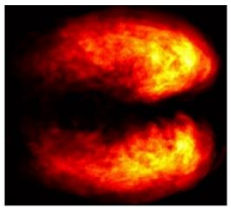

Fig 3: Localization of regions prone to more infection.

2.2 Radiological Scoring:

The two assessment metrics used in the radiological scoring are geographic extent and opacity extent. i.e., for geographic extent, the extent of lung involvement by ground-glass opacity or consolidation of each lung (with the right and left lung scored separately) is scored as 0 = no involvement; 1 = 75% involvement. The scores are then added together, and the total geographic extent score ranges from 0 to 8 (right + left lung). For opacity extent, the degree of opacity is: 0 = no opacity; 1 = ground-glass opacity; 2 = mix of consolidation and ground-glass opacity (less than 50% consolidation); 3 = mix of consolidation and ground-glass opacity (more than 50% consolidation); 4 = complete white-out. The scores are similarly added together, and the total opacity extent score ranges from 0 to 8 (right + left lung). The average scores are then calculated by the radiologists and it is used in the training of deep neural networks. The inter-reader agreement assessed by intra-class correlation coefficient was 0.92 (95% CI: 0.91-0.93) for the geographic extent scores, and 0.87 (95% CI: 0.85-0.89) for the opacity extent scores. After radiological scoring, all CXR image data used in this study, underwent data processing to facilitate faster and efficient training. To avoid the deep neural networks from learning irrelevant visual cues while making severity scoring predictions, the top 8% of the CXR data were cropped to remove boundary artifacts and embedded metadata, that contain patients information. Moreover, all CXR image data were resized to the same dimensions to enable the training of the deep neural networks in this study. In the end, the geographic extent scores (with a dynamic range of 0 to 8) and opacity extent scores (with a dynamic range of 0 to 8) were re-mapped to a unified dynamic range from 0 to 1.

III. MODEL DEVELOPMENT

3.1. U-NET:

The U-Net CNN architecture is a fully convolutional network (FCN) that has two main components: a contraction path, also called an encoder, which captures the image information; and the expansion path, also called decoder, which uses the encoded information to create the segmentation output. We used the U-Net CNN architecture with some small changes: we included dropout and batch normalization layers in each contracting and expanding block. These additions aim to improve training time and reduce overfitting. Figure 4 presents our adapted U-Net architecture.

The two main parts of the network's architecture are contractive and expansive. The contracting path consists of several patches of convolutions with filters of size 3 × 3 and unity strides in both directions, followed by ReLU layers. The first path extracts the key features of the input and gives a feature vector of a specific length. The second path pulls information from the contractive path through copying and cropping mechanism, and from the feature vector using up-convolutions, and by successive implementation, it generates an output segmentation map. The linking of the first and the second paths together allows the network to attain highly accurate information from the contractive path, thus generating the segmentation mask as close as possible to the intended output.

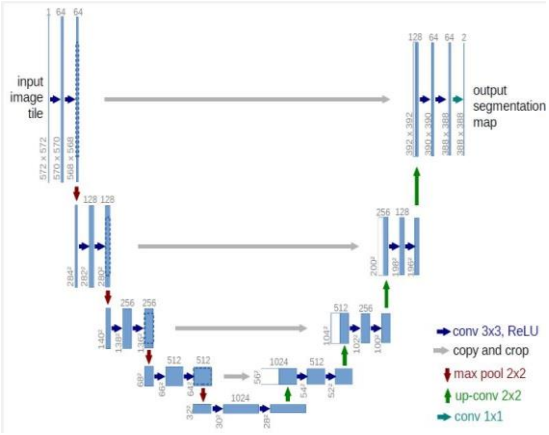

Fig 4: U-NET architecture

CT based lung segmentation using U-net architecture produced optimal results, in comparison with other neural networks. U-Net architecture for multiclass CT medical image segmentation produced far more results than SegNet. The SegNet over performed in binary class medical class CT segmentation variable which is discussed in next section. The U-Net results are noted as follow,

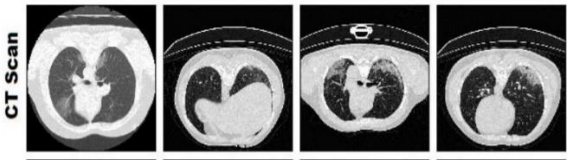

Fig 4.1: CT scan image datasets

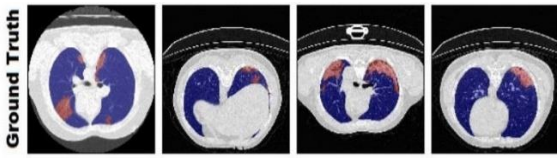

Fig 4.2: Ground Truth images

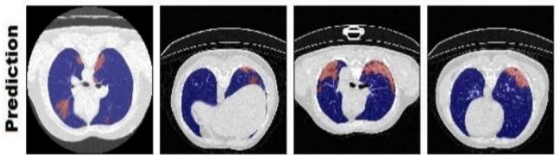

Fig 4.3: U-net Segmentation Results

3.2. SegNet:

SegNet is a Deep Neural Network designed for semantic segmentation. It consists of an encoder and a decoder network. The task requires the network to converge using highly imbalanced datasets since large areas of road images consist of classes such as road, sidewalk, and sky. We demonstrated numerically how the dataset used in this work exhibit disparity in class representation, from the dataset section. Due to this consequence, SegNet was our first choice for this operation. SegNet is a DNN with an encoder-decoder depth of three. The encoder layers are similar to the convolutional layers of the VGG16 network. The decoder constructs the segmentation mask by using pooling indexes from the max-pooling of the corresponding encoder. The creators removed the fully connected layers to reduce complexity, which reduces the number of parameters of the encoder sector from 1.34e+8 to 1.47e+7. The architecture diagram is shown below in figure 5.

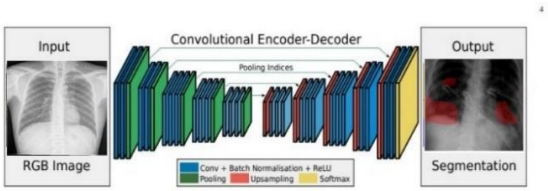

Fig 5: SegNet Architecture using CXR images.

3.3. PSP Net:

In a deep neural network, the size of the receptive field roughly shows how much we use information context. Although the theoretical receptive field of ResNet is already larger than the input image, the empirical receptive field of CNN is much smaller than the latter, especially on higher-level layers. Due to this, many networks do not sufficiently incorporate the momentous global scenery prior. To solve this issue, we propose an effective global level prior representation. Global level average pooling is an efficient baseline model as the global contextual prior, which is generally used in image classification tasks. It was successfully applied to semantic segmentation. But regarding the complex scene images in ADE20K, this strategy will not be enough to cover the necessary information. Pixels in a scene should be annotated on many things and objects. The direct fusion of them, to form a single vector may result in losing the spatial relation and cause ambiguity. Global context along with sub-level region context helps distinguish among various categories. Thus, a more powerful representation could be fused with information from different sub-regions with these receptive fields. A similar result was drawn in the classical work of scene/image classification.

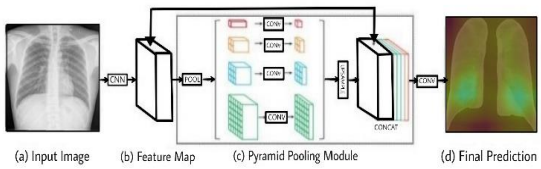

Figure: 6 PSP Net architecture with CT scan images.

IV. RESULTS

4.1. Chest X-ray Evaluation:

To perform lung segmentation, we applied a CNN approach using the U-Net architecture. The U-Net input is the CXR image, and the output is a binary mask that indicates the region of interest (ROI). Thus, the training requires a previously set of binary masks.

The COVID-19 dataset used does not have manually created binary masks for all images. Thus, we adopted a semi-automated approach to creating binary masks for all CXR images. First, we used three additional CXR datasets with binary masks to increase the training sample size and some binary masks provided by v7labs2. We then trained the U-Net model and used it to predict the binary masks for all images in our dataset. After that, we reviewed all predicted binary masks and manually created masks for those CXR images that the model was unable to generalize well. We repeated this process until we judged the result satisfactory and achieved a good intersection between target and obtained regions. U-Net outperformed with higher efficiency which results are discussed as follows.

Table 1 shows the overall U-Net segmentation performance for the test set for each source we used to compose the lung segmentation database considering the Jaccard distance and the Dice coefficient metrics. As we expected, our manually created masks underperformed when compared to the other sources' results, this may have happened because our masks were not made by professional radiologists. Following that, the Cohen v7labs set also presented a somewhat lower performance. Our manual inspection showed that the model did not include the overlapping region between the lung and heart, and the masks in Cohen v7labs included that region, hence the difference. The performance of the remaining databases is outstanding.

Table 1: Lung Segmentation Results

Database	*Jaccard Distance*	*Dice Coefficient*
Cohen v7Labs	0.041 ± 0.027	0.979 ± 0.014
Montgomery	0.019 ± 0.007	0.991 ± 0.003
Shenzhen	0.017 ± 0.008	0.991 ± 0.004
JSRT	0.018 ± 0.011	0.991 ± 0.006
Manually created masks	0.071 ± 0.021	0.964 ± 0.011
Test Set	**0.035** ± 0.027	**0.982** ± 0.014

Table 2 presents F1-Score results for our multi-class scenario. The models using non-segmented CXR images presented better results than the models that used segmented images when we consider raw performance for COVID-19 and lung opacity. Both settings were on par in the normal class.

Table 2: F-1 Score Results

Class	*COVID19*	*Lung opacity*	*Normal*	*Macro avg*
Segmented VGG16	0.83	0.88	0.9	0.87
Segmented ResNet50V2	0.78	0.87	0.91	0.85
Segmented Inception	0.83	0.89	0.92	0.88
Non-segmented VGG16	0.94	0.91	0.91	0.92
Non-segmented ResNet50V2	0.91	0.9	0.92	0.91
Non-segmented InceptionV3	0.86	0.9	0.91	0.9

4.2. CT Evaluation:

Table 3 shows results for both models of binary classifiers after evaluating every experiment of each network. We can see from the results that our networks achieve accuracy values larger than 0.90 in all cases, and 0.954 accuracy in SegNet. PSP-Net performed worse than other two architectures. The standard deviation of experiment 4 is 0.029. The second best network is experiment of the U-NET architecture with an accuracy of 0.95 and a standard deviation of 0.043. The best experiment of each architecture is selected for further performance investigation on the class level. Similarly, we obtain the best experiment for each multi-classification network. The best experiment of the SegNet architecture, giving an accuracy of 0.907 with a standard deviation of 0.06. We also found that the overall best accuracy of 0.908 is achieved by the experiment of U-NET network with a standard deviation of 0.065. All the experiments achieve higher accuracy than 0.8 except for the first three experiments of SegNet.

Table 3: Statistical results for the Binary Segmentor

Net	*Sens*	*Spec*	*Dice*	*G-mean*	*F2*
SegNet	0.956	**0.9542**	**0.749**	0.955	**0.861**
U-Net	0.964	0.948	0.733	**0.956**	0.856

V. DISCUSSION

In this study, we hypothesised that computer-aided deep learning algorithms can accurately predict infection severity on CXRs and CT scan associated with COVID-19 against expert chest radiologist ground level check-up, and the results of the study support this hypothesis. Results from the stratified Monte Carlo cross-validation experiments showed that the learned Covid I-Net deep neural networks could achieve mean R2 between predicted scores and radiologist scores for geographic extent and opacity extent greater than 0.5 when evaluated for 100 different subsets of CXR and CT data. Severity scoring for COVID-19 has gained recent attention due to the rise and continued spread of the COVID-19 across the globe, and the need to find the severity of an infected patient is crucial for determining the best course of action regarding treatment and care. The researchers introduced a scoring scheme for severity analysis of COVID-19 by adapting and simplifying the Radiographic Assessment of lungs, where each lung was divided into three zones (a total of six zones for a human) and each zone was assigned a binary score based on opacity, with the final severity score being the collection of the scores from the different zones. Borghesi and Maroldi27 introduced a scoring scheme where similar to Toussie et al., each lung was divided into three zones, but each zone was instead assigned a score ranging 0 - 3 based on interstitial and alveolar infiltrates. Considering the massive number of infected patients and the radiologists that are needed to analyse them, the use of artificial intelligence-enabled automated severity scoring has strong potential to assist in clinical workflow efficiency given the situation.

VI. CONCLUSION

In this paper, the performance of two deep learning networks (SegNet, U-NET, and PSP Net) was compared in their ability to detect diseased areas in medical images of the lungs of COVID-19 patients. The results demonstrated the ability of the SegNet network to distinguish between infected and healthy tissues in these images. A comparison of these two networks was also performed in multiple infected areas in lung images. The results showed the U-net network's ability to distinguish between these areas outperforms PSP Net. The results obtained in this paper represent promising prospects for the possibility of using deep learning to assist in an objective diagnosis of COVID-19 disease through CT and CXR images of the lung.

REFERENCES

[1] Cohen, J. P., Morrison, P. & Dao, L. COVID-19 image data collection. arXiv 2003.11597 (2020). 7/8

[2] Chung, A. Figure 1 COVID-19 chest x-ray data initiative. https://github.com/agchung/Figure1-COVID-chestxray-dataset (2020).

[3] Chung, A. Actualmed COVID-19 chest x-ray data initiative. https://github.com/agchung/Actualmed-COVID-chestxraydataset (2020).

[4] S., Z., Y., W., T., Z. & L., X. CT features of coronavirus disease 2019 (COVID-19) pneumonia in 62 patients in Wuhan, China. Am J Roentgenol. (2020).

[5] M., C., A., B. & X., M. CT imaging features of 2019 novel coronavirus (2019-nCoV). Am J Roentgenol. (2020).

[6] Ai, T. et al. Correlation of Chest CT and RT-PCR Testing in Coronavirus Disease 2019 (COVID-19) in China: A Report of 1014 Cases. Radiology 200642 (2020).

[7] Fang, Y. et al. Sensitivity of chest CT for covid-19: Comparison to RT-PCR. Radiology 200432 (2020).

[8] Shi, H. et al. Radiological findings from 81 patients with COVID-19 pneumonia in Wuhan, China: a descriptive study. Lancet Infect Dis 20, 425–434 (2020).

[9] Gunraj, H., Wang, L. & Wong, A. COVIDNet-CT: A tailored deep convolutional neural network design for detection of COVID-19 cases from chest CT images. Front. Medicine DOI: 10.3389/fmed.2020.608525 (2020).

[10] Gunraj, H., Sabri, A., Koff, D. & Wong, A. Covid-net ct-2: Enhanced deep neural networks for detection of covid-19 from chest ct images through bigger, more diverse learning. arXiv (2021).

[11] Hemdan, E.E.D., Shouman, M.A., Karar, M.E.: Covidx-net: A framework of deep learning classifiers to diagnose covid-19 in x-ray images. arXiv preprint arXiv:2003.11055 (2020)Google Scholar

[12] Liu, X., Wang, D.: A spectral histogram model for textonmodeling and texture discrimination. Vision Research 42(23), 2617–2634 (2002)PubMedGoogle Scholar

[13] Narin, A., Kaya, C., Pamuk, Z.: Automatic detection of coronavirus disease (covid-19) using x-ray images and deep convolutional neural networks. arXiv preprint arXiv:2003.10849 (2020)Google Scholar

[14] Ozturk, T., Talo, M., Yildirim, E.A., Baloglu, U.B., Yildirim, O., Acharya, and U.R.: Automated detection of covid-19 cases using deep neural networks with x-ray images. Computers in Biology and Medicine p. 103792 (2020) Google Scholar

[15] Sethy, P.K., Behera, S.K.: Detection of coronavirus disease (covid-19) based on deep features. Preprints 2020030300, 2020 (2020)Google Scholar

[16] Simonyan, K., Zisserman, A.: Very deep convolutional networks for large-scale image recognition. arXiv preprint arXiv:1409.1556 (2014)Google Scholar

[17] Song, Y., Zheng, S., Li, L., Zhang, X., Zhang, X., Huang, Z., Chen, J., Zhao, H., Jie, Y., Wang, R., et al: Deep learning enables accurate diagnosis of novel coronavirus (covid-19) with ct images. medRxiv (2020)Google Scholar

[18] Szegedy, C., Liu, W., Jia, Y., Sermanet, P., Reed, S., Anguelov, D., Erhan, D., Vanhoucke, V., Rabinovich, A.: Going deeper with convolutions. In: Proceedings of the IEEE conference on computer vision and pattern recognition. pp. 1–9 (2015)Google Scholar

[19] Wang, L., Wong, A.: Covid-net: A tailored deep convolutional neural network design for detection of covid-19 cases from chest x-ray images. arXiv preprint arXiv:2003.09871 (2020)Google Scholar

[20] Wang, S., Kang, B., Ma, J., Zeng, X., Xiao, M., Guo, J., Cai, M., Yang, J., Li, Y., Meng, X., et al: A deep learning algorithm using ct images to screen for corona virus disease (covid-19). MedRxiv (2020)Google Scholar

[21] Xu, X., Jiang, X., Ma, C., Du, P., Li, X., Lv, S., Yu, L., Ni, Q., Chen, Y., Su, J., et al: A deep learning system to screen novel coronavirus disease 2019 pneumonia. Engineering (2020)Google Scholar

[22] Zhang, B., Zhang, L., Zhang, L., Karray, F.: Retinal vessel extraction by matched filter with first-order derivative of gaussian. Computers in biology and medicine 40(4), 438–445 (2010)PubMedGoogle Scholar

[23] Zhao, J., Zhang, Y., He, X., Xie, P.: Covid-ct-dataset: a ct scan dataset about covid-19. arXiv preprint arXiv:2003.13865 (2020)Google Scholar

[24] Zheng, C., Deng, X., Fu, Q., Zhou, Q., Feng, J., Ma, H., Liu, W., Wang, X.: Deep learning-based detection for covid-19 from chest ct using weak label. medRxiv (2020)Google Scholar